Coherent Phonon Manipulation using Single-mode Circular Electrostatic Resonator

Hongyu Chen[1], Dongyang Chen[1], Ronghua Huan[2], Yongqing Fu[3] and Jin Xie[1,*]
[1]*State Key Laboratory of Fluid Power and Mechatronic Systems, Zhejiang University, Hangzhou 310027, China*
[2]*Department of Mechanics, Key Laboratory of Soft Machines and Smart Devices of Zhejiang Province, Zhejiang University, Hangzhou 310027, People's Republic of China*
[3]*Faculty of Engineering and Environment, University of Northumbria, Newcastle upon Tyne NE1 8ST, UK*
*Email: xiejin@zju.edu.cn

Coherent phonon manipulation is the mechanical analogy to photonic frequency combs while there is lack of a comprehensive evaluation system on the performance. In this paper, coherent phonon manipulation is demonstrated using a single-mode circular electrostatic resonator. Its manipulation mechanism for controlling phononic frequency comb (PFC) parameters is verified experimentally and also theoretically based on waveform derivation of the differential equations. The spacing of PFC system is regulated solely by the pump frequency and a spacing resolution of 0.1 Hz is achieved at room temperature. The amplitude modulation law is investigated and a complete PFC evolution process with a pump threshold of 2 mV_{pp} is achieved. The sweeping experiment of electrostatic resonators is explained from the perspective of phonons. Additionally, feasibility of manipulating phonons using the electrostatic resonators is verified through nonlinearity modulation and damping loss experiments. This new methodology of phonon manipulation can be extended to other resonant energy carriers, with great potentials for frequency detection and phonon-quantum computing.

Key words: Phonon manipulation; Frequency comb; Intramodal coupling; Spacing resolution; Pump threshold.

Significant attention has been paid to the quantum phenomena of frequency combs based on various micro- or nano-devices. An optical frequency comb (OFC) [1]–[7] is an optical spectrum signal with a series of equally spaced frequencies, which can be applied to various applications, such as time calibration, and frequency measurement [8]. As lattice displacement, the collective stimulation of phonons enable further analog research with photons in the electromagnetic field [9]–[11]. A phonon is a collective excitation of the modes of vibrations for elastic materials and phononic frequency combs (PFCs) can be generated by manipulating phonons, and can be applied in applications such as frequency tracking [12], phononic enlargement, quantum computing [13]–[15], phonon amplifiers [16], energy harvesting [17][18],and combing cryptography. Therefore, PFCs are being investigated extensively for both theoretical research and applications.

Currently, the phase-coherent PFCs are generated on Fermi-Pasta-Ulam (FPU) chain [19][20], and multi-modal coupling [12] is commonly employed for comb generation, particularly using piezoelectric devices. A multimodal parametric coupled PFC has been demonstrated using piezoelectric double-ended free beams [21]–[24], and its spacing, energy level, density, comb stability and excitation conditions has been investigated. However, the coupling effect between density and width of combs was found to cause significant challenge of single parameter modulation, as well as Duffing nonlinearity in the modulation between spacing and power level [21]. On the other hand, the spacing is determined quantitatively by the difference between the resonant frequency and the excitation frequency. However, there are significant challenges in practical applications of PFCs because their manufacturing errors often result in variations in the resonant frequency of individual devices. In addition, the applied bulk acoustic wave (BAW) resonator [25] must be carried out at an ultralow temperature of 20 mK, and also had a limited bandwidth for excitation frequency variation (±1.5 Hz), both of which restricted the range of dynamic phononic manipulation. Regarding to using the quartz resonator [26], a linear relationship between the spacing and energy level can be maintained, but the range is limited to ~kHz levels and is also unadjustable. For the nano-electromechanical system (NEMS) device reported in Ref. [27], the combs were modulated quantitatively by the thermal transduction from fiction force which can be too weak and unstable to generate combs for micro-scale devices.

A new modulation method for PFC generation by a simple single-mode circular electrostatic resonator (SCER) is presented in this study to figure out the manipulation mechanism of comb parameters and drive PFCs more effectively and controllably. For this method, the order and spacing of PFC can be independently controlled and are not affected by manufacturing process. Furthermore, the nature of this new PFC is verified through the performance evaluation using the resonator.

Generally, electrostatic resonators are adjusted by using statically tunable electrostatic forces [28]–[30]. The area of the resonance curve envelope can be considered as the phonon storage cavity, where a higher resonance amplitude is corresponding to a greater number of phonons stored. Phonon cavity modulation through this static manipulation is unidirectional. Due to the existing pull-in effect of the electrodes, the manipulation range of static adjustment is limited (**Supplementary Information**). For the SCER shown in FIG. 1(a), the alternating force, as the excitation source, is represented by a combination of DC bias V_{DC} and AC excitation V_d. Since there is no energy coupling between different modes, the effective modulation is only achieved from intra-mode coupling [31]. The intra-mode coupling is provided by an alternating pump signal, causing a change in the equivalent

stiffness and affecting the displacement. The first-order coefficient of vibration displacement is an important parameter to realize the modulation of phonon cavity, including pump frequency and pump intensity [31][32]. The mechanism of coherent phonon frequency comb generation can be written using the following equation from the perspective of excitation of the resonator [31][33]:

$$\ddot{x}+\varsigma\dot{x}+\omega_n^2 x+\tau\cos(\omega_p t)x=F_d\cos(\omega_d t+\phi)+F_l \qquad (1)$$

where $\tau\cos(\omega_p t)$ is the intra-mode coupling term for dynamic stiffness modulation, ϕ is the phase difference between harmonic driving and pump signal, and F_l is thermal Langevin force, which is so weak that can be ignored in this study.

Since the dynamic modulation involves two independent frequency parameters, i.e., the pump frequency and the excitation frequency, a rotational wave approximation [31] is introduced for the solution of Eq. 1. Similar to the expression of photonic waves, the dynamic vibration of displacement field is considered as a linear superposition of *m*-order waves [34],

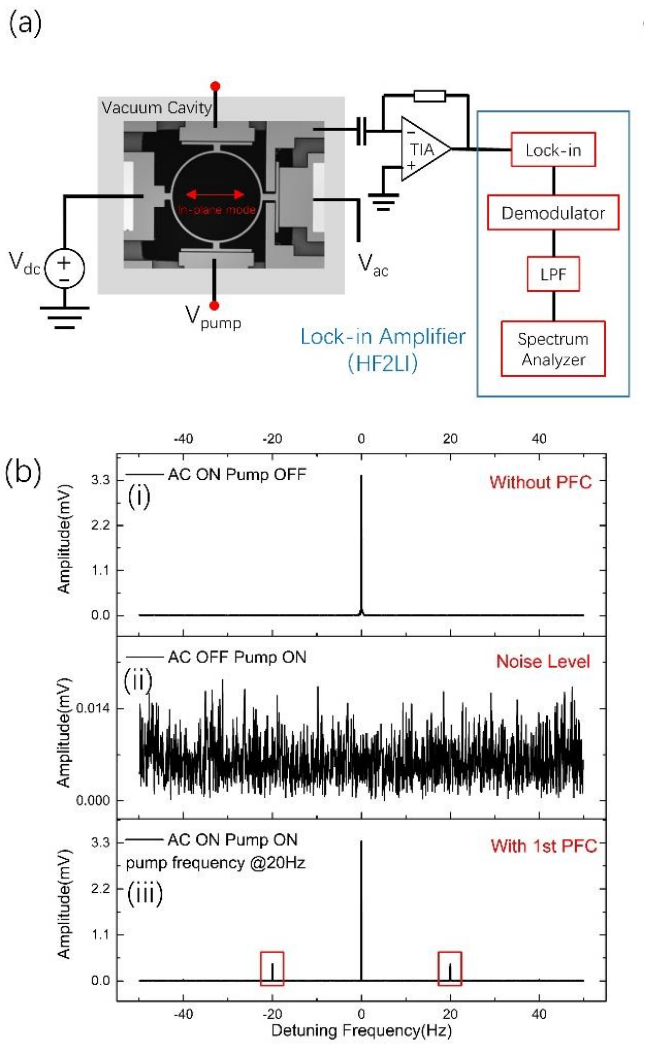

FIG. 1. (a) Schematic diagram of the frequency-locked demodulation experimental platform with the optical microscope image of the SCER designed to exhibit in-phane mode (selected by modulating the frequency of excitation). (b) Environmental test of the electrostatic resonator generating phononic frequency comb.

and if only the real part of displacement field is preserved, then we can obtain the resonant displacement as following:

$$f(x,t)=\mathrm{Re}\left[\sum_{m=-\infty}^{+\infty}A_m(t)e^{i(\omega_d+m\omega_p)t}\right] \qquad (2)$$

where Re is the real part, *m* is the order number. The exponent is expressed as the frequency of each component, and has a corresponding intensity of A_m. In theory, a vibratory displacement field attached to a mechanical resonator can generate combs similar to those from the optical field. Under the pump modulation, the output signal of the resonator is discrete and has equal spacing lines in the frequency spectrum. The spacing is uniquely modulated by the pump frequency. After injection, the phonon group is dynamically pumped to generate a series of cascaded four-wave mixing (FWM) [11][15], and thus the sidebands are generated around the driving frequency (i.e., the center frequency) with the pump frequency as the spacing unit.

The displacement term is substituted into the Eq. 1. After simplification, the differential equation with the amplitude of waves A_m is obtained [31].

$$\left[2i(\omega_d+m\omega_p)+\varsigma\right]\dot{A}_m+\left[-\left(\omega_d+m\omega_p\right)^2+i\varsigma(\omega_d+m\omega_p)+\omega_n^2\right]A_m +\frac{\Gamma}{2}A_{m+1}+\frac{\Gamma}{2}A_{m-1}=F_d e^{i\delta}\delta_{m,0} \qquad (3)$$

The right side of Eq. 3 is the Dirac function. The driving force only exists at the excitation frequency and does not have a direct excitation effect on the series of waves. The side waves are generated through FWM instead of direct resonant driving. Eq. 3 is a conceptual equation of a series of equations where the comb lines with different orders have different amplitudes, phases and driving forces corresponding to the orders. A series of spectral lines can form a comb which has frequency clarity and can be compared to an OFC as a frequency ruler.

A modulation environment experiment was firstly carried out and is illustrated in FIG. 1(a). At room temperature, when the pump signal is turned off, the output signal in FIG. 1(bi) shows a pure harmonic at the excitation frequency, indicating a static manipulation. When only the pump signal is injected without the excitation signal, there is only noise in the spectrum as shown in FIG. 1(bii). This is because the resonator is not in the resonant oscillation and the injected phonon group cannot generate the PFCs. Only when the resonator is in the resonant oscillation and the dynamic parametric pump is injected, the PFCs can be formed through phonon mixing, as shown in FIG. 1(biii). These results indicate that the phonon cavity can modulate the effective dynamic range and that the resonant-state material lattice is the primary condition for phonon manipulation. The demodulated output signals are filtered and then the comb lines are formed. Overall, this experiment shows that the alternating pump signal is necessary for generating PFCs and that the resonator must be in the resonant oscillation for phonon mixing to occur. The results confirm the mechanism of phonon manipulation in PFC generation.

For the PFCs, a precise spacing between discrete lines is essential among all the related parameters. In Eq. 2, the real component of the output signal comprises a sequence of waves, with frequency being modified by the excitation frequency and pump frequency. Firstly, the effects of pump frequency are studied on the open-loop frequency sweep and frequency-

locked demodulation, respectively. The frequency sweep was performed as in the static modulation, and then the pump frequency was changed step by step as shown in FIG. 2(a). The spacing is the frequency interval between the center frequency peak and first-order comb lines. The measurement error, including that of data sampling and noise interference, is about 3%. As the pump frequency is decreased, the degree of aliasing among cavities becomes more serious. By adjusting the pump frequency, the phonon modulation range (i.e. the cavity bandwidth) can be increased. However, there exists a trade-off where the comb spacing is submerged after cavity aliasing. Here the effective cavity bandwidth is defined as the pump

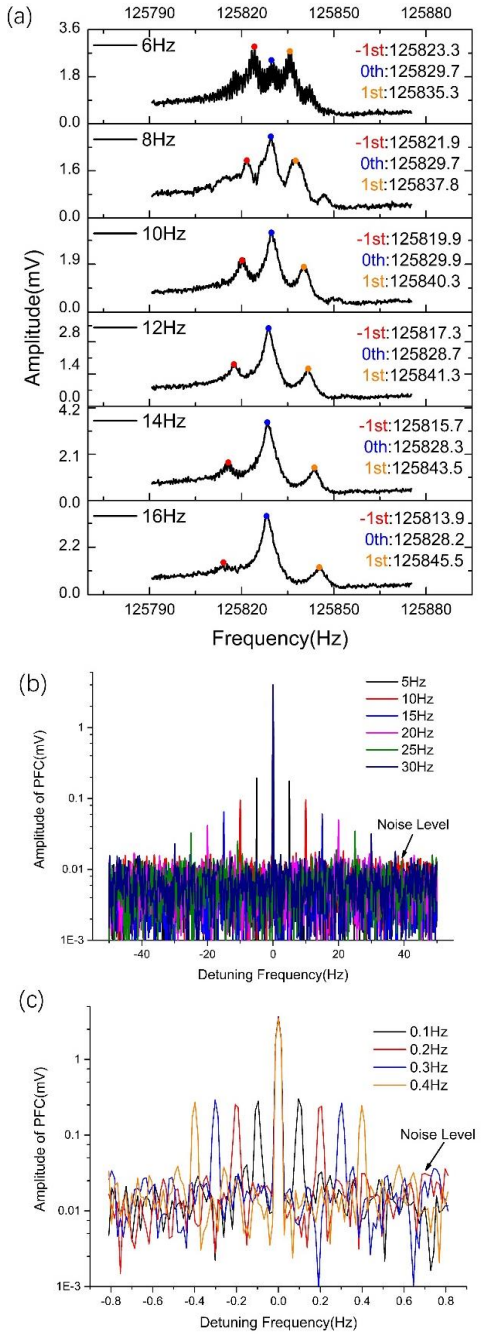

FIG. 2. The open-loop frequency sweep curves of the resonator under the pump frequency change from 6 Hz to 16 Hz. The spectrum diagram of the demodulated signal under the pump frequency change (5 Hz is the step size for (b) while 0.1 Hz for (c)).

frequency at which phonon cavity aliasing occurs. The smaller the cavity bandwidth, the lower the effective threshold for comb modulation. The modulation bandwidth is correlated with the quality factor (Q). A low modulation threshold and also an extensive range of phonon manipulation can be developed by a high-Q resonator. On the other hand, phonon cavity aliasing can broaden the bandwidth of the resonator, enabling the high-Q resonators to operate within a larger bandwidth. As the pump frequency is increased, the amplitude of central comb is gradually increased, whereas the amplitude of the first-order comb lines decreases. Based on the theory of energy conversion, under a constant pump intensity, a higher pump frequency results in more energy carried by a phonon, and thus a smaller quantity of phonons will be generated. Under this situation, the coupling effect is weakened, resulting in a reduction in the amplitude of sidebands. The pump frequency manipulates the energy-mixing ratio in each order of the PFC. A small pump frequency induces aliasing between the comb cavity, converting the energy from the center comb to the high-order combs. The intuitive performance can be shown in a reduction in the output voltage of central comb on the frequency curve , which can also be explained using the multiple-scale method [10][34][35]. (**Shown in the Supplementary Information**)

As shown in FIG. 2(b), an increase in spacing is observed between the first-order combs and the center frequency when the pump frequency is increased with a 5 Hz increment at room temperature. The amplitude of the comb lines decreases as the

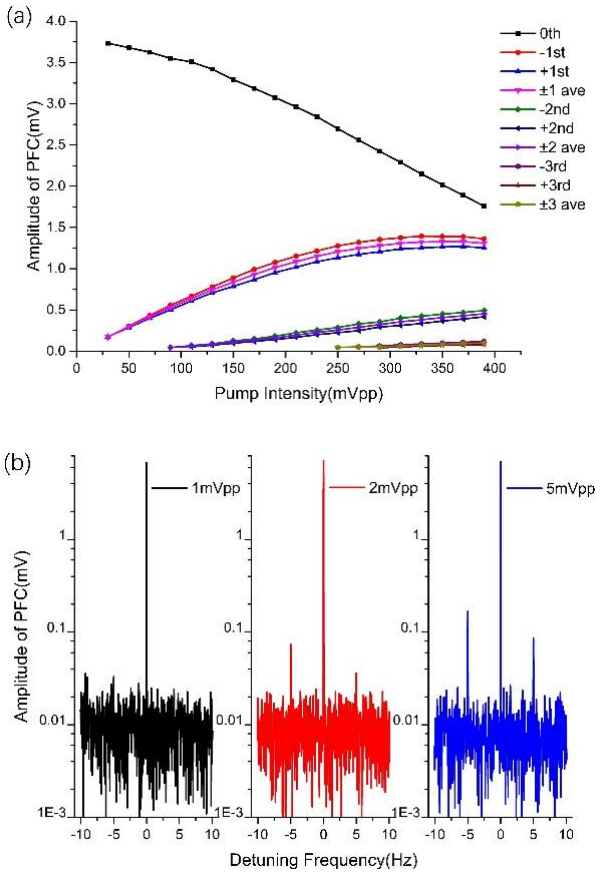

FIG. 3. (a) The diagram of the PFC evolution process, including the energy proportion and the stepwise evolution of the comb lines. (b) The pump threshold intensity experiment for pump frequency of 5 Hz

spacing increases while the pump intensity remains a constant, also aligning with the multiple-scale method. The resolution of PFC is another crucial parameter for applications like frequency measurement and frequency-time transformation. A frequency step of 0.1 Hz is employed in this study, ranging from 0.1 Hz to 0.4 Hz. Precise spacings remain visible in FIG. 2(c). The comb with a frequency resolution of 0.1 Hz can be achieved, revealing the high level of accuracy of the PFCs, which can enhance the dynamic range of frequency measurement and be applied for sensing small frequency signals. The first-order combs observed in the sweep curve can be attributed to the phonon injection with a fixed pump frequency. The energy is centered at the excitation frequency, and the pump frequency is equal to the spacing, producing a local resonance of Rabi oscillation [36]. It is worth mentioning that the high quality of combs is an advantage of intramodal mixing, as the spacing only depends on the frequency of pump signal. The frequency can be controlled using a highly accurate signal function generator. In contrast, comb generators based on intermodal mixing have spacing that depends on the relationship between various modes. The frequency of mode state is often inaccurate, influenced by manufacturing error.

As is well known, there are certain requirements for pump intensity in OFCs. Specifically. when the intensity is below a threshold value, photon entanglement will occur. Otherwise, the FWM Kerr combs will be generated. Similarly, PFCs also exhibit a certain threshold. By varying the pump intensity, the amplitudes of the center and side bands were recorded at room temperature and plotted as shown in FIG. 3(a). The amplitude of sidebands increases with increasing pump intensity, whereas that of the center (0th) frequency band decreases. When the pump intensity becomes higher, more phonon groups are introduced into the cavity, and thus phonon storage becomes more significant than its consumption, leading to a gradual increase in the amplitude of the side combs at a specific spacing. Consistent with the energy transfer law in the OFCs, the energy conversion between the center and side frequency band becomes more intense as the amplitude of the sideband is increased, thus resulting in the flow of energy from center frequency to the sidebands. Ultimately, the sidebands reach another dynamic balance between phonon storage and consumption.

In addition, there are several dramatic changes of the order of combs as shown in FIG. 3(a). As the pump intensity is continuously increased, higher-order sidebands are produced. For the high-order sidebands, the energy characteristics described above are also fitted in the region where the order does not change. The amplitude of the higher-order comb lines is typically smaller than that of the lower-order ones, meaning that the high-order comb lines are produced by the FWM based on the low-order combs. Consequently, the energy of the high-order combs is smaller than that of the low-order comb lines, which is consistent with the mechanism of the first-order comb generation. Since the energy of the center band accounts for the largest proportion among all of the bands, a reduction in the energy of the first-order and second-higher-order comb lines is from the generation of the higher-order comb lines. A new dynamic balance between energy storage and consumption is then established. This is also the reason why the phonon manipulation cannot generate or jump to a certain higher order comb. Phonons change their energy levels step by step under the external conditions.

After the mechanism of pump intensity is clarified, we then analyzed the minimum pump intensity of comb generation, also called pump threshold intensity. FIG. 3(b) shows these results under different pump intensities. When the pump intensity is as small as 1 mV_{pp}, only one signal exists at the excitation frequency, and noise is observed in all other frequency region. Sidebands are not produced or drowned out by noise. When the pump intensity is increased to the threshold value (i.e., 2 mV_{pp}), the sidebands are generated at spacing of the pump frequency besides the center frequency. As the pump intensity is increased to 5 mV_{pp}, the amplitude of combs is continuously increased, which is similar to the phenomena in the discussion on the

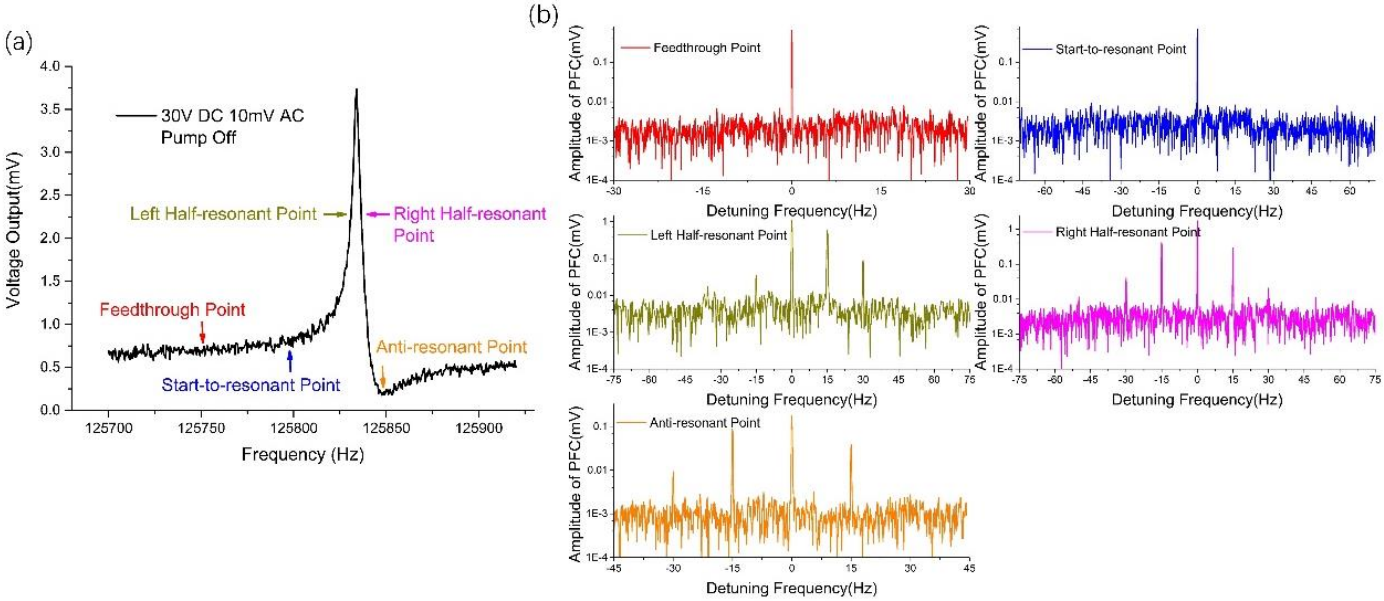

FIG. 4. (a) The sweep curve with five points, including feedthrough level, start-to-resonant point, left and right half-resonant peaks, anti-resonant point. (b) Frequency comb distribution of different points at pump frequency of 15 Hz.

pump intensity. A comb generator with a low pump threshold has the potential application in sensing weak frequency signals.

The open-loop sweep curve is also analyzed from the perspective of phonics as shown in FIG. 4. Five representative points were selected, covering the feedthrough region [37], half-peak resonant region and anti-resonant peak. Then the spectral features were obtained through frequency-locked demodulation. Firstly, at the fixed pump frequency of 15 Hz, the combs with different amplitudes and orders are generated in the frequency domain, but the spacing remains stable. This verifies that spacing is manipulated only by pump frequency, which is easier to operate than the coupling effect in the piezoelectric cantilever devices. On the other hand, through the spectral lines at points of feedthrough level and start-to-resonance, the electrostatic resonator has a certain range for comb modulation. The range of comb modulation is determined by the resonator's performance at different excitation frequencies, and the resonant peak is the most efficient point for phonon storage and comb generation. As the energy is decreased, the storage of phonons becomes weaker, resulting in a single spectral line without phononic mixing, and the intensity is corresponding to the amplitude of the point. At the points on both sides of the peak, high-order comb lines appear, and the amplitudes of the center band are relatively high. Regarding to the anti-resonant point, although high-order comb lines appear in the spectrum, these amplitudes are small. Therefore, by independently selecting the excitation region, different comb states can be generated, such as high-order combs, the first-order comb, and a single resonance peak, which have the potential application on combing cryptography. So far, the experimental results demonstrate that the envelope formed by the sweep curve is related to the spectral comb of each point. The amplitude of each point is equivalent to the peak intensity in the spectrum, so the spectrum comb is also a feedback of resonance.

In order for phonon manipulation based on the SCER, the essence of phonon manipulation needs to be proven as the modulation of mechanical resonant motion, which is the characteristic of resonators. The higher-order comb has also its resonant characteristics, similar to that of the center resonance. Linearity can be determined by the forward and backward bidirectional sweep curves. Linearity is essentially an energy state of resonator system [38]–[40]. The resonator can be regarded as an energy carrier, and its performance depends on the energy level state. As shown in FIG. 5(a), when the resonator works in the linear situation, the pump intensity is increased stepwise to generate high-order sidebands. Both the sidebands and the center resonance work linearly. From the view of energy, the comb modulation is simpler in the linear region than that in the nonlinear state. The linearity of each order comb is consistent with the initial state of the resonator, but there is a phenomenon of linearity change caused by energy

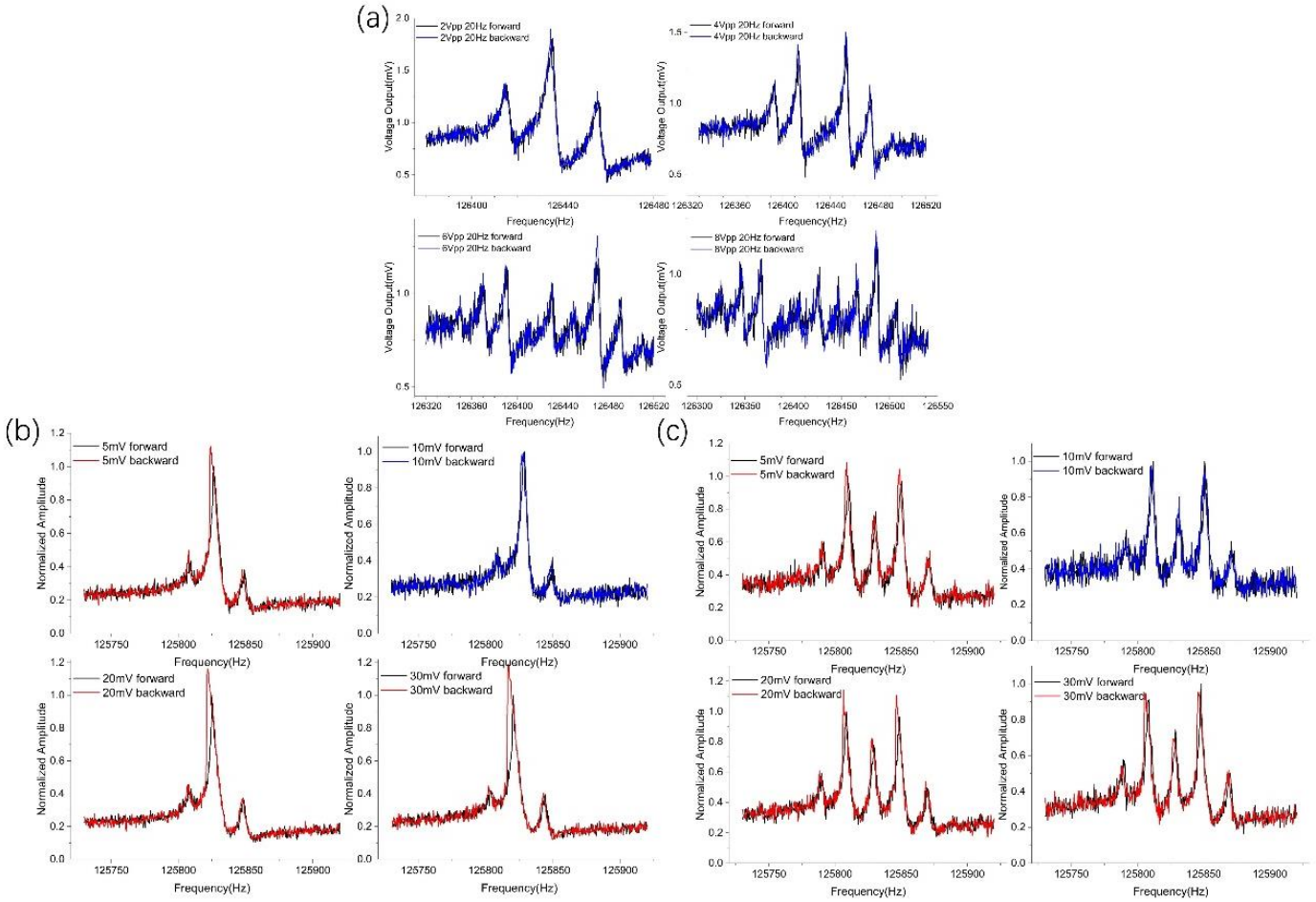

FIG. 5. The evolution process of the phonon cavity working in the linear state (blue curves) (a) with different pump intensity from 2 V_{pp} to 8 V_{pp}, and the nonlinear state (red curves), in which the states include two types: (b) single-order and (c) high-order.

conversion in the nonlinear state. Next, to change the initial working state, the alternating excitation intensity was changed from 5 mV to 30 mV, so that the resonator continuously worked among the linear and nonlinear regions. The obtained sweeping frequency curves are shown in FIGs. 5(b) and (c). A 700 mV_{pp}, 20 Hz pump signal was introduced for the first-order generation as shown in FIG. 5(b). In the nonlinear state, hysteresis appears at the center curve while the first-order curves are overlapped. At this time, a small amount of energy at the center frequency is converted to the first-order comb, making that the center comb energy account for a relatively large proportion and still in a nonlinear state. Meanwhile, the first-order comb retains a linear state because the energy has not yet reached the nonlinear level.

In order to study the resonant characteristics of the higher-order combs, the pump intensity was further increased to 2 V, and the obtained higher-order phonon curves are shown in FIG. 5(c). Since the high-order phonon cavity was obtained by converting FWM energy, the proportion of energy was mainly transferred from the center frequency to the first order comb. Nonlinearity of the first-order sidebands is clearly observed. Hysteresis is due to changes in the systemic performance after energy accumulation. Specifically, low energy levels correspond to linear regions. When the energy level crosses the linear boundary, the system enters a state of nonlinear oscillation, resulting in the nonlinear weakening of the center band and the nonlinear enhancement of the first-order sidebands. Throughout the energy conversion process, when the energy at the center frequency is converted into the higher-order energy bands, the nonlinear characteristics experience degradation to the linear region, resulting in a decrease of the phonon cavity modulation bandwidth and amplitude ratio. The phonon probability density distribution is directly related to the mechanical vibration intensity, so the essence of coherent phonon manipulation is the regulation of mechanical resonance.

The optoelectrical resonator often displays a linear loss of refractive index [5], which is resulted from the material of the microcavity and waveguide dispersion. Similarly, the mechanical resonator of the PFC experiences energy loss from air damping [28] and structural dissipation. Structural dissipation can essentially decrease the threshold for comb generation, i.e., the half-peak bandwidth is reduced. Here the impact of air damping is examined. As the pressure is increased gradually, the energy loss becomes larger, so the phonon consumption is increased. The amplitudes of comb lines at various air pressures are displayed in FIG. 6(a). The resonant motion is affected by the energy consumption of air damping,

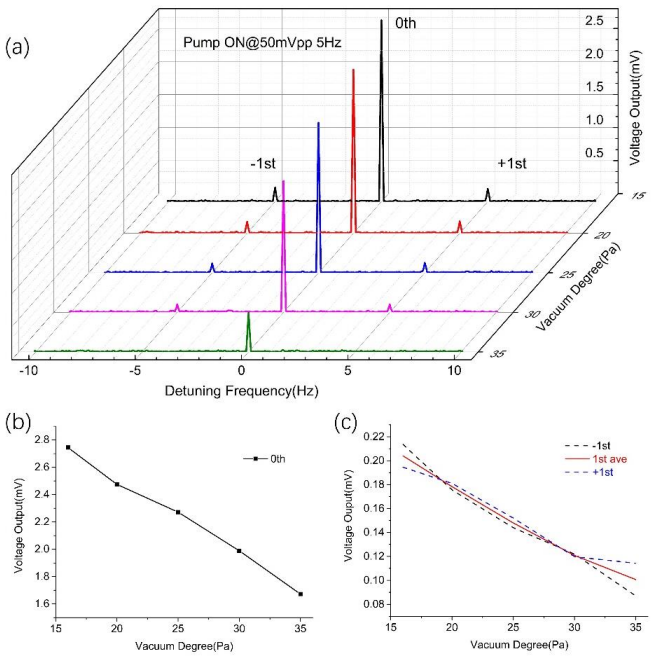

FIG. 6. Frequency comb resonance characteristic with the pump strength of 50 mV_{pp} and frequency of 5 Hz at room temperature. (a) The spectrogram of comb lines under different vacuum degrees. (b) The amplitude changes of the center frequency peak and (c) the first-order sideband.

causing the amplitude at center frequency to decrease with increasing air pressure as shown in FIG. 6(b). As the energy of the center band decreases, the energy conversion between the center and first-order frequency bands is also weakened, further reducing the amplitude of the sidebands in FIG. 6(c). Thus, the essence of sidebands is the mechanical resonant motion so that resonators can be controlled as phonon cavities. The linearity modulation of the frequency sweep curve and the damping-to-intensity experiment both demonstrate PFC manipulation based on the electrostatic resonators.

To access the generation and derivation process of PFCs, six different aspects are considered for performance, i.e., operation environment (RT for room temperature, AP for atmospheric pressure), excitation threshold, spacing resolution, comb orders, and method of generation. The comparisons with the state-of-art PFCs are listed in Table 1. Results showed that the proposed PFC based on SOI-manufactured electrostatic resonator exhibits advanced comprehensive performance.

Table 1: Comparisons with the state-of-art PFCs

Year	Device	Temperature	Vacuum Degree	Threshold Power	Spacing Limitation	Order	Method
2019 [41]	AlN Disk	RT	AP	50 mV	2 kHz	3rd @350mV	2-mode parametric pump
2022 [42]	2-coupled SOI	RT	Vacuum	100 mV	15 Hz	3rd @4V	1:3 internal resonance
2018	2-coupled	RT	AP	100 mV	3 kHz	<3rd miss	2-mode mixing pump

[21]	AlN beams						
2018 [43]	CC single nonlinear beam	RT	Vacuum	600 mV	0.5 Hz	<10th miss	1:3 internal resonance
2018 [23]	3-coupled AlN beams	RT	AP	69 V	~kHz	3rd @69V	2-mode 3-wave mixing
2016 [44]	FF single AlN beam	RT	AP	707 mV	0.12 MHz	1st-2nd	Intrinsic localized to phonon modes
2017 [24]	FF single AlN beam	RT	AP	2.24 V	2.6 kHz	3rd @2.37V	3-wave mixing
2020 [26]	High-Q quartz resonator	10~22 ℃	Vacuum	45.7 V	5.4 kHz	Up to 6th	Series resonance
2016 [45]	3 RF resonator	RT	Vacuum	10 V_{pp}	>3 kHz	Only 1st	Intermodal coupling
2013 [31]	Coupled NEMS	1.5K	0.05 mPa	0.5 V_{pp}	0.11 kHz	High order miss	Multi-wave phonon mixing
2020 [25]	BAW quartz	20 mK	3*10^{-6} mbar	2*10^{-4} mV_{pp}	0.7~2Hz	1st jump to 11th	Antiresonace and strong nonlinearity
Our work	SCER	RT	7~10 Pa	2 mV_{pp}	0.1 Hz	Cover 1st to high	Intra-modal pump mixing

In summary, this paper presents a novel approach for coherent phonon manipulation utilizing an electrostatic single-mode circular resonator at room temperature. The study reveals several parameter laws of PFC modulation. The pump frequency modulates the comb spacing, and the pump intensity affects both comb order and energy distribution. A comb spacing resolution of 0.1 Hz is achieved, and only a pump intensity of 2 mV_{pp} is required to excite a first-order comb. Furthermore, the phonon storage is affected by different working states of the resonator. The feasibility of PFC modulation is validated using a MEMS resonator to perform nonlinearity modulation and air damping experiments. The methodology of coherent phonon manipulation based on intra-modal mixing can be further extended to other resonators, which has important application potentials such as frequency detection, frequency tracking, phonon quantum computing, thermal-phonon interaction, and entanglement of phonons.

Data availability

The datasets generated during and/or analyzed during the current study are available from the corresponding authors on reasonable request.

Acknowledgements

This work is supported by the "National Natural Science Foundation of China (52175552)" and the "Zhejiang Provincial Natural Science Foundation of China (LZ19E050002)". The authors most gratefully acknowledge Dr. Jiabao Sun of ZJU Micro-Nano Fabrication Center for his professional and enthusiastic assistance during MEMS fabrication.

[1] T. Udem, R. Holzwarth, and T. W. Hänsch, "Optical frequency metrology," *Nature*, vol. 416, no. 6877, pp. 233–237, 2002, doi: 10.1038/416233a.

[2] N. Picqué and T. W. Hänsch, "Frequency comb spectroscopy," *Nat. Photonics*, vol. 13, no. 3, pp. 146–157, 2019, doi: 10.1038/s41566-018-0347-5.

[3] T. J. Kippenberg, R. Holzwarth, and S. A. Diddams, "Microresonator-based optical frequency combs," *Science (80-.).*, vol. 332, no. 6029, pp. 555–559, 2011, doi: 10.1126/science.1193968.

[4] P. Del'Haye, A. Schliesser, O. Arcizet, T. Wilken, R. Holzwarth, and T. J. Kippenberg, "Optical frequency comb generation from a monolithic microresonator," *Nature*, vol. 450, no. 7173, pp. 1214–1217, 2007, doi: 10.1038/nature06401.

[5] Y. K. Chembo, "Kerr optical frequency combs: Theory, applications and perspectives," *Nanophotonics*, vol. 5, no. 2, pp. 214–230, 2016, doi: 10.1515/nanoph-2016-0013.

[6] A. Leshem, Z. Qi, T. F. Carruthers, C. R. Menyuk, and O. Gat, "Thermal instabilities, frequency-comb formation, and temporal oscillations in Kerr microresonators," *Phys. Rev. A*, vol. 103, no. 1, pp. 1–12, 2021, doi: 10.1103/PhysRevA.103.013512.

[7] Z. Qi, G. D'Aguanno, and C. R. Menyuk, "Nonlinear frequency combs generated by cnoidal waves in microring resonators," *J. Opt. Soc. Am. B*, vol. 34, no. 4, p. 785, 2017, doi: 10.1364/josab.34.000785.

[8] N. R. Newbury, "Searching for applications with a fine-tooth comb," *Nat. Publ. Gr.*, vol. 5, no. April, 2011, doi: 10.1038/nphoton.2011.38.

[9] M. Hase, M. Katsuragawa, A. M. Constantinescu, and H. Petek, “Frequency comb generation at terahertz frequencies by coherent phonon excitation in silicon,” vol. 6, no. April, pp. 1–5, 2012, doi: 10.1038/nphoton.2012.35.

[10] Z. Wang, “Nonlinearity-mediated digitization and amplification in electromechanical phonon-cavity systems,” pp. 2–9, 2022, doi: 10.1038/s41467-022-29995-x.

[11] M. L. Gorodetsky and T. J. Kippenberg, “Kerr-frequency combs in microresonators,” vol. 6, no. July, 2012, doi: 10.1038/nphoton.2012.127.

[12] A. Ganesan and A. Seshia, “Resonance tracking in a micromechanical device using phononic frequency combs,” *Sci. Rep.*, vol. 9, no. 1, pp. 1–7, 2019, doi: 10.1038/s41598-019-46003-3.

[13] M. Blencowe, “Quantum electromechanical systems,” *Phys. Rep.*, vol. 395, no. 3, pp. 159–222, 2004, doi: 10.1016/j.physrep.2003.12.005.

[14] L. Wang and B. Li, “Thermal logic gates: Computation with phonons,” *Phys. Rev. Lett.*, vol. 99, no. 17, pp. 1–4, 2007, doi: 10.1103/PhysRevLett.99.177208.

[15] D. Hatanaka, I. Mahboob, K. Onomitsu, and H. Yamaguchi, “Mechanical random access memory in a phonon circuit,” 2014.

[16] I. S. Grudinin, H. Lee, O. Painter, and K. J. Vahala, “Phonon laser action in a tunable, two-level system,” *Opt. InfoBase Conf. Pap.*, pp. 12–13, 2010.

[17] X. Le, Q. Shi, P. Vachon, E. J. Ng, and C. Lee, “Piezoelectric MEMS - Evolution from sensing technology to diversified applications in the 5G/Internet of Things (IoT) era,” *J. Micromechanics Microengineering*, vol. 32, no. 1, 2022, doi: 10.1088/1361-6439/ac3ab9.

[18] J. Zhu *et al.*, “Development trends and perspectives of future sensors and MEMS/NEMS,” *Micromachines*, vol. 11, no. 1, 2020, doi: 10.3390/mi11010007.

[19] T. Dauxois, “Fermi, Pasta, Ulam, and a mysterious lady,” *Phys. Today*, vol. 61, no. 1, pp. 55–57, 2008, doi: 10.1063/1.2835154.

[20] G. M. Chechin, N. V. Novikova, and A. A. Abramenko, “Bushes of vibrational modes for Fermi-Pasta-Ulam chains,” *Phys. D Nonlinear Phenom.*, vol. 166, no. 3–4, pp. 208–238, 2002, doi: 10.1016/S0167-2789(02)00430-X.

[21] A. Ganesan, C. Do, and A. Seshia, “Excitation of coupled phononic frequency combs via two-mode parametric three-wave mixing,” *Phys. Rev. B*, vol. 97, no. 1, pp. 1–6, 2018, doi: 10.1103/PhysRevB.97.014302.

[22] A. Ganesan, C. Do, and A. Seshia, “Observation of phononic frequency combs in a micromechanical resonator,” *2017 Jt. Conf. Eur. Freq. Time Forum IEEE Int. Freq. Control Symp. EFTF/IFC 2017 - Proc.*, pp. 148–152, 2017, doi: 10.1109/FCS.2017.8088829.

[23] A. Ganesan and A. Seshia, “Coexistence of multiple multimode nonlinear mixing regimes in a microelectromechanical device,” *Appl. Phys. Lett.*, vol. 112, no. 8, 2018, doi: 10.1063/1.5009705.

[24] A. Ganesan, C. Do, and A. Seshia, “Phononic Frequency Comb via Intrinsic Three-Wave Mixing,” *Phys. Rev. Lett.*, vol. 118, no. 3, pp. 1–5, 2017, doi: 10.1103/PhysRevLett.118.033903.

[25] M. Goryachev, S. Galliou, and M. E. Tobar, “Generation of ultralow power phononic combs,” *Phys. Rev. Res.*, vol. 2, no. 2, pp. 1–7, 2020, doi: 10.1103/PhysRevResearch.2.023035.

[26] R. L. Kubena, W. S. Wall, J. Koehl, and R. J. Joyce, “Phononic comb generation in high-Q quartz resonators,” *Appl. Phys. Lett.*, vol. 116, no. 5, 2020, doi: 10.1063/1.5128930.

[27] M. I. Dykman, G. Rastelli, M. L. Roukes, and E. M. Weig, “Resonantly Induced Friction and Frequency Combs in Driven Nanomechanical Systems,” *Phys. Rev. Lett.*, vol. 122, no. 25, p. 254301, 2019, doi: 10.1103/PhysRevLett.122.254301.

[28] H. Chen, D. Chen, Z. Shi, R. Huan, and J. Xie, “A MEMS frequency modulation electrometer based on pre-bias charge mechanism to enhance performance,” *J. Micromechanics Microengineering*, vol. 32, no. 10, 2022, doi: 10.1088/1361-6439/ac8685.

[29] D. Chen, Y. Wang, X. Chen, W. Huang, and J. Xie, “Duffing Nonlinearity Localization via Extension Energy Confinement in an Elastic Mode Semicircular Beams Resonator,” *IEEE Electron Device Lett.*, vol. 40, no. 2, pp. 314–317, 2019, doi: 10.1109/LED.2018.2889468.

[30] J. E. Lee, B. Bahreyni, and A. A. Seshia, “Sensors and Actuators A : Physical An axial strain modulated double-ended tuning fork electrometer,” vol. 148, pp. 395–400, 2008, doi: 10.1016/j.sna.2008.09.010.

[31] H. Okamoto *et al.*, “Coherent phonon manipulation in coupled mechanical resonators,” *Nat. Phys.*, vol. 9, no. 8, pp. 480–484, 2013, doi: 10.1038/nphys2665.

[32] I. Mahboob, K. Nishiguchi, H. Okamoto, and H. Yamaguchi, “Phonon-cavity electromechanics,” *Nat. Phys.*, vol. 8, no. 5, pp. 387–392, 2012, doi: 10.1038/nphys2277.

[33] Z. Qi, C. R. Menyuk, J. J. Gorman, and A. Ganesan, “Existence conditions for phononic frequency combs,” *Appl. Phys. Lett.*, vol. 117, no. 18, pp. 5–10, 2020, doi: 10.1063/5.0025314.

[34] M. C. Cross, A. Zumdieck, R. Lifshitz, and J. L. Rogers, “Synchronization by nonlinear frequency pulling,” *Phys. Rev. Lett.*, vol. 93, no. 22, pp. 1–4, 2004, doi: 10.1103/PhysRevLett.93.224101.

[35] Q. Yang *et al.*, “Asymmetric phononic frequency comb in a rhombic micromechanical resonator,” *Appl. Phys. Lett.*, vol. 118, no. 22, 2021, doi: 10.1063/5.0044039.

[36] D. Zhu *et al.*, “Coherent Phonon Rabi Oscillations with a High-Frequency Carbon Nanotube Phonon Cavity,” *Nano Lett.*, vol. 17, no. 2, pp. 915–921, 2017, doi: 10.1021/acs.nanolett.6b04223.

[37] D. Chen *et al.*, “Feedthrough parasitic nonlinear resonance in micromechanical oscillators,” *Appl.*

Phys. Lett., vol. 117, no. 13, 2020, doi: 10.1063/5.0018696.

[38] X. Wang, X. Wei, D. Pu, and R. Huan, "Single-electron detection utilizing coupled nonlinear microresonators," *Microsystems Nanoeng.*, vol. 6, no. 1, pp. 0–6, 2020, doi: 10.1038/s41378-020-00192-4.

[39] D. Chen, J. Sun, M. Pandit, G. Sobreviela, and X. Chen, "ELASTIC MODE SEMICIRCULAR BEAMS RESONATOR OSCILLATOR WITH WEAKENED NONLINEARITIES State Key Laboratory of Fluid Power and Mechatronic Systems , Zhejiang University , CHINA Nanoscience Centre , University of Cambridge , UNITED KINGDOM National University o," *2019 20th Int. Conf. Solid-State Sensors, Actuators Microsystems Eurosensors XXXIII (TRANSDUCERS EUROSENSORS XXXIII)*, no. June, pp. 2091–2094, 2019.

[40] D. Wagg, *Nonlinear Vibration with Control*. .

[41] M. Park and A. Ansari, "Formation, evolution, and tuning of frequency combs in microelectromechanical resonators," *J. Microelectromechanical Syst.*, vol. 28, no. 3, pp. 429–431, 2019, doi: 10.1109/JMEMS.2019.2898003.

[42] Y. Xu and J. E. Y. Lee, "Single-device and on-chip feedthrough cancellation for hybrid MEMS resonators," *IEEE Trans. Ind. Electron.*, vol. 59, no. 12, pp. 4930–4937, 2012, doi: 10.1109/TIE.2011.2180274.

[43] D. A. Czaplewski *et al.*, "Bifurcation Generated Mechanical Frequency Comb," *Phys. Rev. Lett.*, vol. 121, no. 24, p. 244302, 2018, doi: 10.1103/PhysRevLett.121.244302.

[44] A. Ganesan, C. Do, and A. Seshia, "Observation of intrinsic mode splitting in a standalone micromechanical resonator," *2016 IEEE Int. Freq. Control Symp. IFCS 2016 - Proc.*, pp. 8–11, 2016, doi: 10.1109/FCS.2016.7546787.

[45] H. Okamoto *et al.*, "A strongly coupled Λ-type micromechanical system," *Appl. Phys. Lett.*, vol. 108, no. 15, pp. 1–5, 2016, doi: 10.1063/1.4945741.